Image-guided, Tumor Stroma-targeted ^{131}I Therapy of Hepatocellular Cancer After Systemic Mesenchymal Stem Cell-mediated NIS Gene Delivery

Kerstin Knoop[1], Marie Kolokythas[1], Kathrin Klutz[1], Michael J. Willhauck[1], Nathalie Wunderlich[1], Dan Draganovici[2], Christian Zach[3], Franz-Josef Gildehaus[3], Guido Böning[3], Burkhard Göke[1], Ernst Wagner[4], Peter J. Nelson[2] and Christine Spitzweg[1]

[1]Department of Internal Medicine II, Ludwig-Maximilians-University, Munich, Germany; [2]Clinical Biochemistry Group, Medical Policlinic, Ludwig-Maximilians-University, Munich, Germany; [3]Department of Nuclear Medicine, Ludwig-Maximilians-University, Munich, Germany; [4]Department of Pharmacy, Center of Drug Research, Pharmaceutical Biology-Biotechnology, Ludwig-Maximilians-University, Munich, Germany

Due to its dual role as reporter and therapy gene, the sodium iodide symporter (NIS) allows noninvasive imaging of functional NIS expression by ^{123}I-scintigraphy or ^{124}I-PET imaging before the application of a therapeutic dose of ^{131}I. NIS expression provides a novel mechanism for the evaluation of mesenchymal stem cells (MSCs) as gene delivery vehicles for tumor therapy. In the current study, we stably transfected bone marrow–derived CD34$^-$ MSCs with NIS cDNA (NIS-MSC), which revealed high levels of functional NIS protein expression. In mixed populations of NIS-MSCs and hepatocellular cancer (HCC) cells, clonogenic assays showed a 55% reduction of HCC cell survival after ^{131}I application. We then investigated body distribution of NIS-MSCs by ^{123}I-scintigraphy and ^{124}I-PET imaging following intravenous (i.v.) injection of NIS-MSCs in a HCC xenograft mouse model demonstrating active MSC recruitment into the tumor stroma which was confirmed by immunohistochemistry and *ex vivo* γ-counter analysis. Three cycles of systemic MSC-mediated NIS gene delivery followed by ^{131}I application resulted in a significant delay in tumor growth. Our results demonstrate tumor-specific accumulation and therapeutic efficacy of radioiodine after MSC-mediated NIS gene delivery in HCC tumors, opening the prospect of NIS-mediated radionuclide therapy of metastatic cancer using MSCs as gene delivery vehicles.

Received 9 July 2010; accepted 15 April 2011; published online 17 May 2011. doi:10.1038/mt.2011.93

INTRODUCTION

Mesenchymal stem cells (MSCs) are pluripotent progenitor cells with high proliferative and self renewal capacity, which play a key role in maintenance and regeneration of diverse tissues based on their ability to differentiate into cells of connective tissue lineages, including bone, fat, cartilage and muscle.[1–3] In the course of tissue injury, or during chronic inflammation, MSCs can contribute to tissue remodeling by their mobilization and subsequent recruitment to the site of injury. While the exact mechanisms by which circulating progenitor cells home to remodeling tissues remain unclear, it is thought that chemokine biology and integrins underlie tissue-specific homing of stem cells.[4,5]

Tumors are composed of malignant tumor cells and the "benign" tumor stromal compartment that includes blood vessels, infiltrating inflammatory cells, extracellular matrix, and stromal fibroblasts. This tumor stroma plays a key role in tumor growth, tumor angiogenesis and metastatic potential of a tumor, and has therefore become an important target for tumor therapy.[1,2] The process of tumor stroma formation is similar to that seen in wound healing which results in tissue remodeling with recruitment and high proliferation of mesenchymal cells. We and others have shown that MSCs are actively recruited to growing tumor stroma where they differentiate into diverse tumor stroma-associated cell types including cells that comprise the tumor vasculature and stromal fibroblast-like cells.[1,3,4,6–8] Based on their intrinsic tumor homing capacity, MSCs have gained attention as potential vehicles for delivering therapeutic genes to tumor environments after systemic application, potentially providing a means to deliver therapeutic genes not only to the primary tumor, but also to tumor metastases. A series of recent reports have provided the proof of principle of MSC-mediated gene delivery demonstrating successful tumor-selective engraftment of *ex vivo* transduced MSCs.[1,7–11]

Sodium iodide symporter (NIS), an intrinsic transmembrane glycoprotein with 13 putative transmembrane domains, is responsible for the ability of thyroidal cells to concentrate iodide, the first and rate-limiting step in the process of thyroid hormonogenesis, which can be effectively blocked by the competitive inhibitor perchlorate ($NaClO_4$).[12,13] Due to its expression in follicular cell-derived thyroid cancer cells, NIS provides the molecular basis for the diagnostic and therapeutic application of radioiodine, which

Correspondence: *Christine Spitzweg, Klinikum der Universitaet Muenchen-Campus Grosshadern, Medizinische Klinik II, Marchioninistrasse 15, 81377 Munich, Germany. E-mail: Christine.Spitzweg@med.uni-muenchen.de*

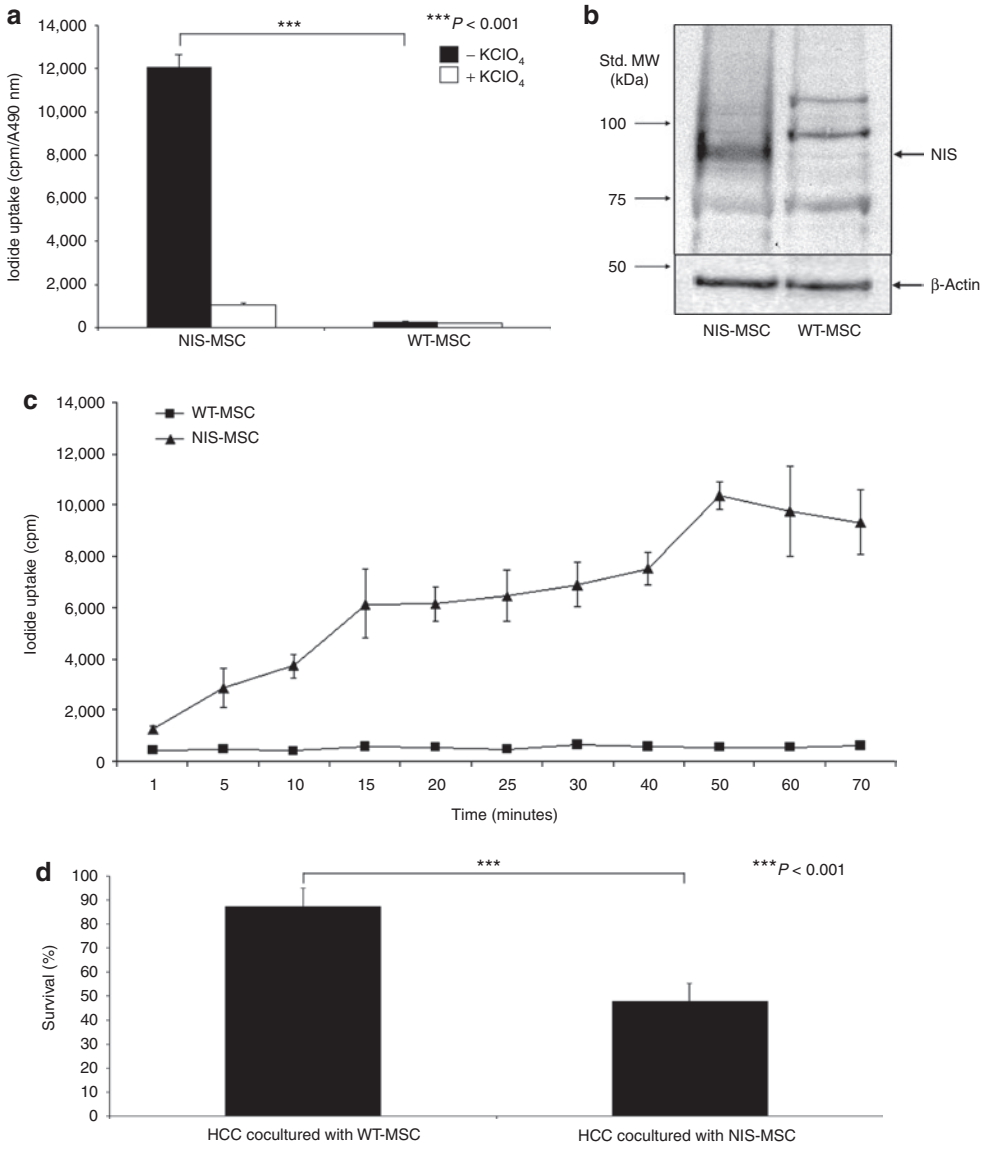

Figure 1 ***In vitro*** **analysis of mesenchymal stem cells (MSCs) stably expressing the sodium iodide symporter (NIS).** (**a**) ^{125}I uptake was measured in NIS-MSCs compared to wild-type (WT)-MSCs. NIS-MSCs showed a 12-fold increase in perchlorate-sensitive ^{125}I accumulation. In contrast, no perchlorate-sensitive iodide uptake above background level was observed in WT-MSCs ($P < 0.001$). (**b**) Analysis of NIS protein expression in NIS-MSCs as compared to WT-MSCs by western blot analysis. NIS protein was detected as a major band of a molecular mass of 80–90 kDa which was not detected in WT-MSCs. MW, molecular weight. (**c**) Time course of iodide uptake in NIS-MSCs and WT-MSCs. Iodide accumulation reached half-maximal levels in NIS-MSCs within 10–15 minutes and became saturated at 40–50 minutes, while WT-MSCs showed no iodide accumulation. (**d**) In an *in vitro* clonogenic assay mixed populations of WT-MSCs and hepatocellular cancer (HCC) cells as well as NIS-MSCs and HCC cells (ratio 1:1) were exposed to 29.6 MBq ^{131}I. In HCC cells cocultured with NIS-MSCs a 55% reduction of cell survival was measured, whereas HCC cells cocultured with WT-MSCs survived the ^{131}I incubation to almost 100% ($P < 0.001$). Results represent means of three plated cell densities ± SD (100, 500 and 1,000 cells per well).

has been successfully used for more than 70 years for the treatment of thyroid cancer patients, and represents the most effective form of systemic anticancer radiotherapy available today.[12] Since its cloning in 1996, the *NIS* gene has been identified and characterized as a therapeutic gene for the treatment of thyroidal or extrathyroidal tumors following selective *NIS* gene transfer into tumor cells. This allows the therapeutic application of radioiodine and alternative radionuclides, such as ^{188}Re and ^{211}At.[12–15] *NIS* also represents one of the most promising reporter genes available, which allows direct noninvasive imaging of functional NIS expression by ^{123}I-scintigraphy and ^{124}I-PET imaging, as well as exact dosimetric calculations before proceeding to therapeutic application of ^{131}I.[12,16,17] *NIS* has many characteristics of an optimal reporter and therapy gene, as it is a nonimmunogenic protein with a well-defined body biodistribution and expression, that mediates the transport of readily available radionuclides, such as ^{131}I, ^{123}I, ^{125}I, ^{124}I, ^{99m}Tc, ^{188}Re or ^{211}At.[12,13]

The field of gene therapy has made considerable strides in the last decade through the development of new vector systems, including engineered MSCs, and an increasing repertoire of therapeutic genes. The application of *NIS* in its role as reporter gene allows detailed characterization and direct monitoring of *in vivo* vector biodistribution as well as localization, level, and duration of transgene expression after viral or nonviral gene delivery. These

are recognized as critical elements in the design of clinical gene therapy trials.[12,16,18] Several research groups, including our own, have demonstrated the potential of *NIS* as reporter gene in various applications, demonstrating that *in vivo* imaging of radioiodine accumulation by ^{123}I- or ^{99m}Tc-scintigraphy as well as ^{123}I-SPECT/computed tomography fusion imaging correlates well with the results of *ex vivo* γ-counter measurements as well as NIS mRNA and protein analysis.[19–26] In addition, PET imaging using ^{124}I provides significant advantages for exact localization and quantitative analysis of NIS-mediated radioiodine accumulation due to enhanced resolution and sensitivity.[17,27]

In the current study, we applied MSCs as gene delivery vehicles for tumor-targeted *NIS* gene expression in a hepatoma mouse model. Based on its dual function as reporter and therapy gene, *NIS* was used initially for noninvasive imaging of MSC recruitment and whole body biodistribution as well as localization, level and duration of NIS expression after systemic application of NIS-transduced MSCs. The therapeutic capacity of ^{131}I therapy was subsequently evaluated after systemic administration of NIS expressing MSCs.

RESULTS

In vitro characterization of MSCs stably expressing NIS

After stable transfection of immortalized human bone marrow–derived CD34$^-$ MSCs with a NIS expressing plasmid (CMV-NIS-pcDNA3) (NIS-MSC), the transfected cells showed a 12-fold increase in NIS-mediated iodide uptake activity, which could be blocked upon treatment with the NIS-specific competitive inhibitor perchlorate (**Figure 1a**). In contrast, in wild-type (WT)-MSCs no perchlorate-sensitive iodide uptake above background level was observed.

NIS protein expression in NIS-transfected MSCs was confirmed by western blot analysis using a mouse monoclonal NIS-specific antibody (**Figure 1b**). The antibody recognizes the carboxy-terminus of human NIS and revealed a major band of a molecular mass of approximately 80–90 kDa in NIS-MSCs, which was not detected in WT-MSCs.

A time course of iodide uptake in NIS-MSCs and WT-MSCs showed that in NIS-MSCs, iodide accumulation reached half-maximal levels within 10–15 minutes and became saturated at 40–50 minutes (**Figure 1c**). No NIS-specific iodide accumulation above background level was observed in WT-MSCs.

A clonogenic assay was then performed to determine whether ^{131}I sequestered by NIS-MSCs would be able to kill adjacent hepatocellular cancer (HCC) cells in cocultures through the crossfire effect of ^{131}I (**Figure 1d**). NIS-MSCs or WT-MSCs cocultured with HCC cells were incubated in Hank's balanced salt solution (HBSS) containing 29.6 MBq ^{131}I for 7 hours. HCC cells, cocultured with WT-MSCs (ratio 1:1) showed no significant cell killing after incubation with ^{131}I. In contrast, in cocultures of HCC cells and NIS-MSCs (ratio 1:1), HCC cells, which have no iodide uptake activity *per se*, revealed a 55% reduction in cell survival (**Figure 1d**).

In vivo radioiodine biodistribution studies

In nude mice harboring HCC xenografts 5×10^5 NIS- or WT-MSCs were injected intravenously (i.v.) via the tail vein three times in 4-day intervals. Seventy-two hours following the last MSC injection, 18.5 MBq ^{123}I was administered and radioiodine distribution was monitored using a γ-camera. While no significant iodide accumulation was detected in tumors after application of WT-MSC (**Figure 2c**), significant iodide accumulation was observed in 74 % of Huh7 tumors following NIS-MSC application, in addition to physiologic iodide accumulation in thyroid gland, stomach and bladder (**Figure 2a**). As determined by serial scanning, a

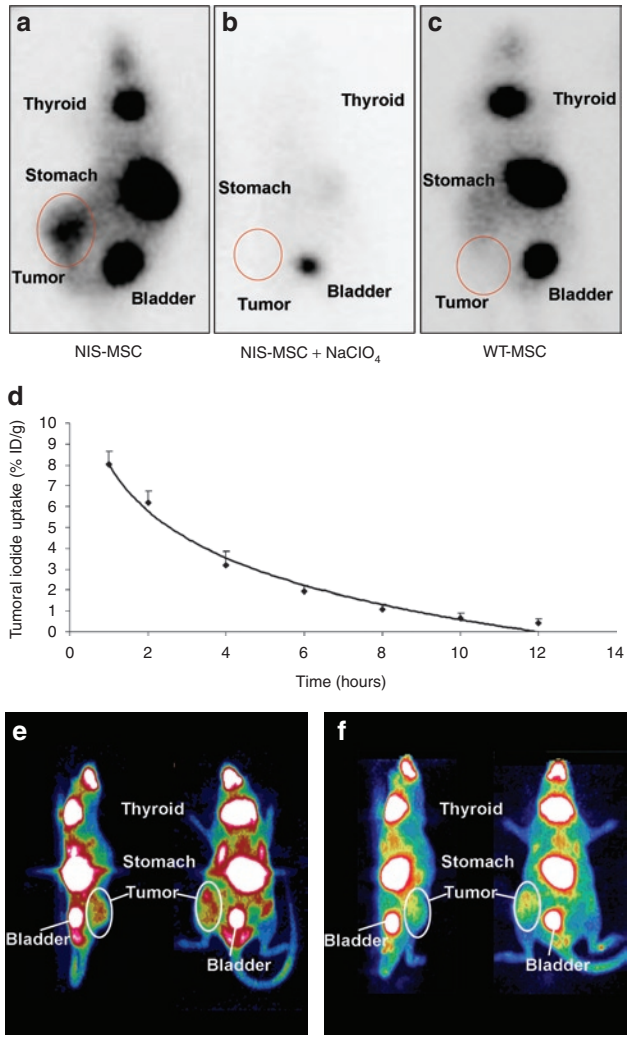

Figure 2 *In vivo* **radioiodine biodistribution studies.** ^{123}I γ-camera imaging of mice harboring Huh7 tumors after mesenchymal stem cell (MSC)-mediated sodium iodide symporter (NIS) gene delivery 3 hours following ^{123}I administration. (**a**) After three intravenous (i.v.) applications of NIS-MSCs significant tumor-specific iodide accumulation was induced (7–9 % ID/g ^{123}I), which was completely abolished upon (**b**) pretreatment with $NaClO_4$. (**c**) In contrast, mice injected with WT-MSCs showed no tumoral iodide uptake. (**a**,**c**) Iodide was also accumulated physiologically in thyroid, stomach and bladder. (**d**) Time course of ^{123}I accumulation in Huh7 tumors after three i.v. NIS-MSC applications followed by injection of 18.5 MBq ^{123}I as determined by serial scanning. Maximum tumoral radioiodine uptake was 7–9% ID/g tumor with an average effective half-life of 3 hours for ^{131}I. (**e**,**f**) ^{124}I PET imaging of mice harboring Huh7 tumors after MSC-mediated NIS gene delivery. After three i.v. applications of NIS-MSCs significant tumor-specific iodide accumulation was confirmed by PET imaging (left: sagittal slice orientation, right: coronal slice orientation).

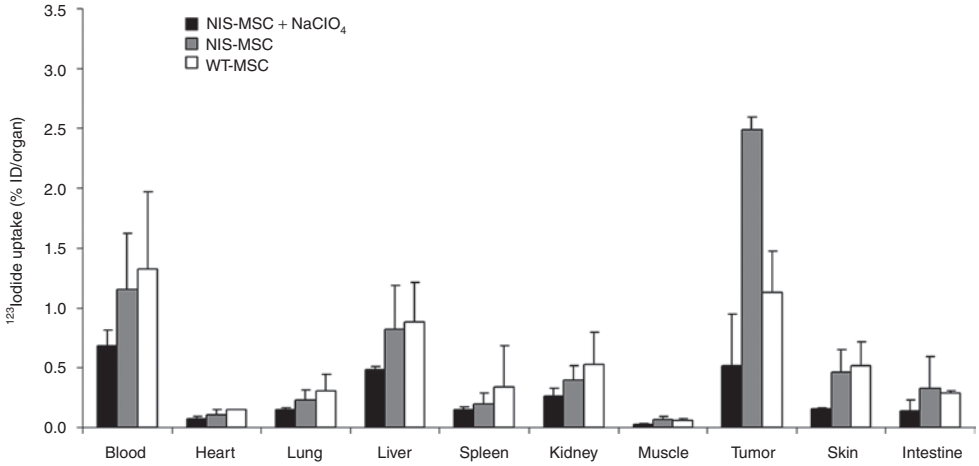

Figure 3 Evaluation of iodide biodistribution *ex vivo* 5 hours following injection of 18.5 MBq ^{123}I. Tumors in NIS-MSC-injected mice showed high perchlorate-sensitive iodide uptake activity (~2.5–3% ID/organ), while no significant iodide accumulation was measured in tumors after injection of WT-MSCs or in nontarget organs. Results are reported as percent of injected dose per organ ± SD.

maximum of ~7–9% ID/g ^{123}I was accumulated after application of NIS-MSCs with a biological half-life of 4 hours. Considering a tumor mass of 1 g and an effective half-life of 3 hours for ^{131}I, a tumor absorbed dose of 43.7 ± 7.7 mGy/MBq ^{131}I was calculated (**Figure 2d**). To confirm that tumoral iodide uptake was mediated by functional NIS expression, a subset of NIS-MSC injected mice received $NaClO_4$ 30 minutes prior to ^{123}I administration. In all experiments, a single injection of 2 mg $NaClO_4$ completely blocked tumoral iodide accumulation in addition to abolishing iodide uptake in stomach and thyroid gland (**Figure 2b**).

In a subset of mice, radioiodine biodistribution was also monitored using ^{124}I-PET imaging after i.v. injection of 20 MBq ^{124}I (**Figure 2e,f**). Three-dimensional data were generated using iterative reconstructions of list-mode data (0–40 minutes), which gave better anatomical definition. Significant tumor-selective iodide accumulation was observed following NIS-MSC application thereby confirming the findings of the planar γ-camera imaging, but allowing a more detailed three-dimensional analysis of tumoral iodide accumulation. One hour after iodide application a maximum tumoral iodide uptake of ~5–7% ID/g was measured.

Ex vivo radioiodine biodistribution studies

Ex vivo biodistribution studies confirmed significant iodide uptake in tumors following three systemic i.v. applications of NIS-MSCs resulting in a tumoral iodide uptake of 2.5–3% ID/organ ^{123}I 5 hours after radioiodine injection. In contrast, mice injected with WT-MSCs showed no significant tumoral iodide uptake. No significant iodide uptake levels were observed in the nontarget organs lung, liver, spleen or kidney (**Figure 3**). In both groups, the thyroid gland and the stomach accumulated ~40% and 39% ^{123}I ID/organ resulting from endogenous expression of NIS in thyroid and stomach. It is important to point out that due to the exquisite regulation of thyroidal NIS expression by thyroid-stimulating hormone, ^{123}I accumulation in the thyroid gland can effectively be downregulated by thyroid hormone treatment as shown in humans.[28] In addition, iodide accumulation in the stomach is mostly a result from pooling of gastric juices, which is more prominent in mouse experiments than usually seen in humans due to the anesthesia for a prolonged period during imaging procedure[12,22] (data not shown). Administration of perchlorate in mice injected with NIS-MSCs significantly blocked iodide uptake in tumors and in physiologically NIS-expressing tissues including thyroid gland and stomach (**Figure 3**).

Analysis of NIS mRNA expression by quantitative real-time PCR

In order to assess the relative NIS mRNA expression after systemic MSC application, mRNA from tumors and control tissues was extracted and analyzed by quantitative real-time PCR with NIS-specific oligonucleotide primers. While low levels of NIS mRNA expression were detected in tumors after WT-MSC administration, significant levels of NIS mRNA were detected in tumors of mice following systemic NIS-MSC injection (**Figure 4**). As expected, administration of the competitive NIS-inhibitor perchlorate had no influence on NIS mRNA expression in tumors treated with NIS-MSCs. In other organs, including liver, lung, kidneys and spleen no significant NIS mRNA expression was observed after systemic NIS-MSC injection.

Immunohistochemical analysis of NIS protein expression in Huh7 tumors

To better determine MSC distribution, tumor specimens were immunohistochemically stained with NIS- and SV40 large T Ag-specific antibodies. SV40 large T Ag was used to immortalize the MSC and could thus be used for *ex vivo* detection of the adoptively transferred MSC. NIS-specific immunoreactivity was detected throughout the tumor stroma with most prominent staining in areas neighboring blood vessels in tumors of mice that were injected with NIS-MSCs (**Figure 5a**, arrows). Distribution of NIS-specific immunoreactivity was similar to the localization of SV40 large T Ag (**Figure 5b**). Lungs, liver, and kidneys showed no detectable NIS or SV40 large T Ag immunoreactivity (data not shown). In contrast, strong accumulation of SV40 large T Ag-expressing cells was observed in the spleens of mice after administration of NIS-MSCs (**Figure 5f**), while no NIS-specific immunoreactivity was detected (**Figure 5e**). WT-MSC-injected

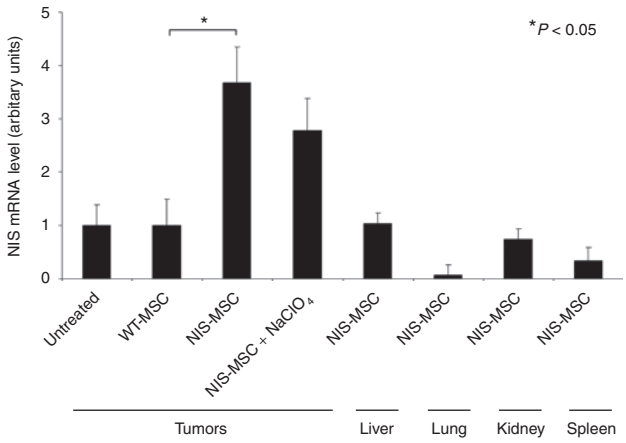

Figure 4 Analysis of sodium iodide symporter (NIS) mRNA expression in Huh7 tumors and nontarget organs by quantitative real-time PCR (qPCR). While only a low background level of NIS mRNA expression was detected in untreated tumors (which was set as one arbitrary unit) or tumors injected with wild-type mesenchymal stem cells (WT-MSC), significant levels of NIS mRNA expression were induced in Huh7 tumors after three applications of NIS-MSCs with or without $NaClO_4$ pretreatment ($P < 0.05$). In addition, no significant NIS mRNA expression was detected in nontarget organs after three applications of NIS-MSCs. Results are reported as NIS/GAPDH ratios.

mice showed no significant NIS protein expression in tumors (**Figure 5c**) and other organs like lungs, liver, kidneys or spleen (**Figure 5g**). However, after WT-MSC application SV40 large T Ag-specific immunoreactivity was widely detectable in implanted Huh7 tumors (**Figure 5d**) as well as in spleen (**Figure 5h**) demonstrating efficient MSC recruitment into the tumor stroma after systemic application. The presence of MSC in the spleen may result either from the direct recruitment of the cells,[6] or from active filtration of the exogenously applied MSC from the peripheral circulation.

Radioiodine therapy studies *in vivo* after MSC-mediated systemic NIS gene transfer

The effect of therapeutic ^{131}I was then evaluated in concert with application of NIS-MSCs. The ^{131}I therapy regime was optimized using small groups of mice ($n = 4$) and showed the best results when mice were treated with three cycles of NIS-engineered MSCs followed by ^{131}I application (data not shown). Mice treated with NIS-MSCs followed by application of saline or mice treated with WT-MSCs followed by application of ^{131}I, or saline treated mice all showed an exponential tumor growth. In contrast, NIS-transduced (NIS-MSCs) and ^{131}I-treated tumors showed a significant delay in tumor growth ($P = 0.001703$ (NaCl) and $P = 0.008103$ (WT-MSC)) (**Figure 6a**). Mice showed no major adverse effects of radionuclide or MSC treatment in terms of lethargy or respiratory failure.

Upon completion of the therapy study, mice were killed and tumors were dissected and processed for immunfluorescence analysis. Immunfluorescence analysis using a Ki67-specific antibody (green) and an antibody against CD31 (red, labeling blood vessels) showed striking differences between mice treated with NIS-MSC/^{131}I (**Figure 6b**) and mice treated with WT-MSC/^{131}I (**Figure 6c**) as well as mice treated with NIS-MSC/NaCl

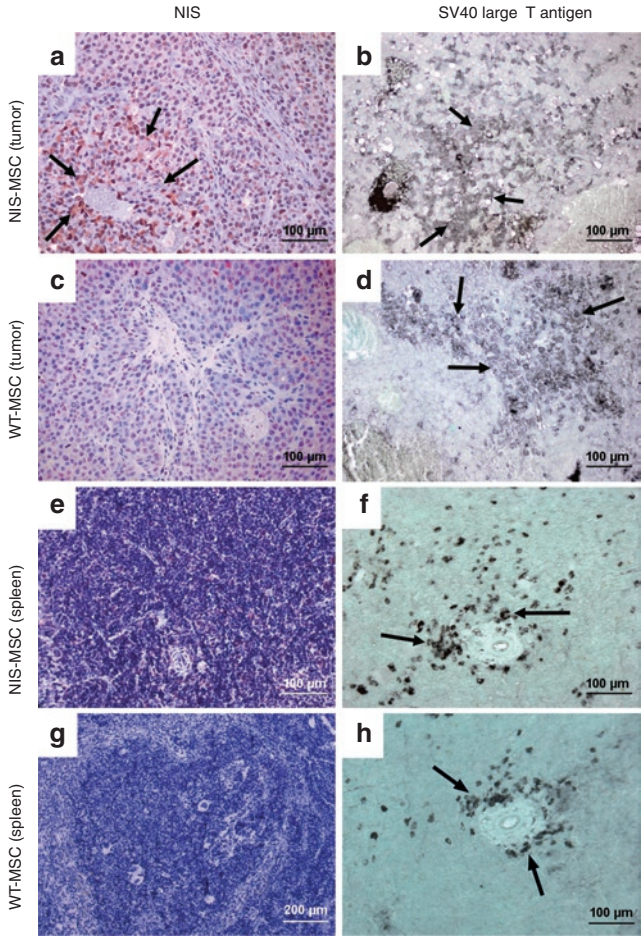

Figure 5 Immunohistochemical staining of Huh7 tumors and spleen after application of NIS-MSCs or WT-MSCs. (**a**) After application of NIS-MSCs Huh7 tumors revealed NIS-specific immunoreactivity throughout the tumor stroma, which was most prominent in the vicinity of blood vessels, (**b**) with a similar distribution of SV40 large T Ag-positive cells. (**c**) After application of WT-MSCs no NIS-specific immunoreactivity was detected in Huh7 tumors, (**d**) while strong cytoplasmic SV40 large T Ag staining was detected, in particular in the vicinity of blood vessels. Other organs like lung, liver, and kidneys showed no detectable NIS protein expression and no SV40 large T Ag staining (data not shown). (**e**–**h**) In contrast, strong accumulation of SV40 large T Ag-expressing cells was detected in the spleen of mice that were injected with (**f**) NIS-MSCs or (**h**) WT-MSC, (**e**,**g**) while no NIS-specific immunoreactivity was detected.

(**Figure 6d**). Control tumors showed a Ki67-index of ~45 ± 8.7% and a mean vessel density of 5 ± 0.45%, whereas tumors treated with NIS-MSC and ^{131}I exhibited a lower intratumoral blood vessel density of 1.85 ± 0.25% and a proliferation index of 25 ± 4.1% after ^{131}I therapy.

DISCUSSION

NIS represents one of the oldest and most successful targets for molecular imaging. Cloning of the *NIS* gene has provided a versatile new reporter and therapy gene which has paved the way for the development of a novel cancer gene therapy strategy based on NIS-mediated radionuclide imaging and therapy.[12,13] In previous studies in a prostate cancer model, we made use of a prostate-specific promoter to drive tissue-specific NIS expression after *ex vivo*

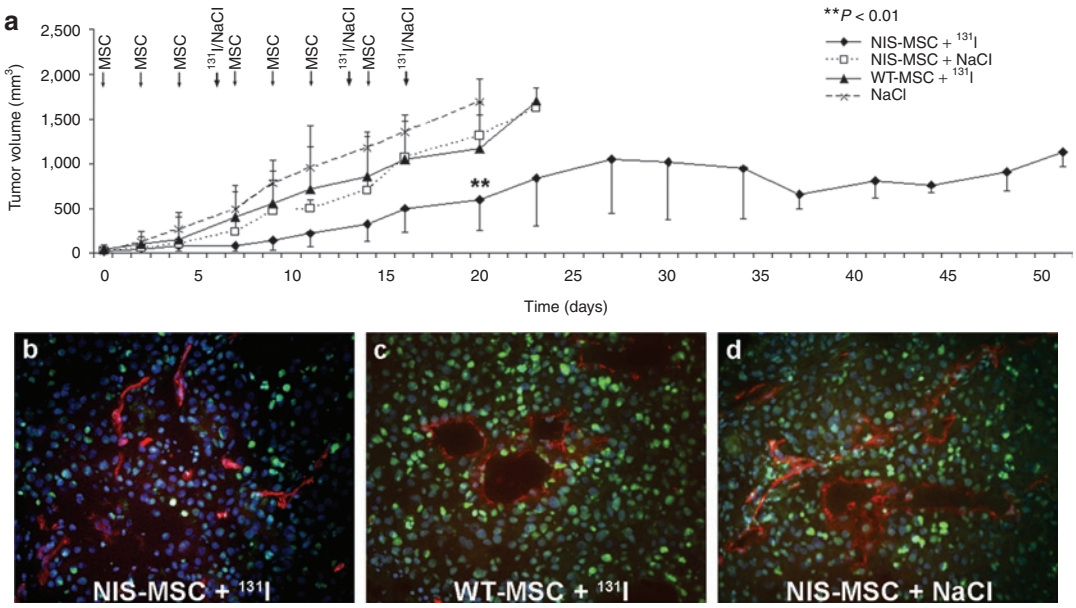

Figure 6 Radioiodine therapy studies *in vivo* after MSC-mediated systemic *NIS* gene transfer. Two groups of mice were established receiving 55.5 MBq ^{131}I 48 hours after the last of three NIS-MSC (n = 15) or wild-type (WT)-MSC (n = 15) applications in 2-day intervals, respectively. This cycle was repeated once 24 hours after the last ^{131}I application. Twenty-four hours after these two treatment cycles, one additional MSC injection was administered followed by a third ^{131}I (55.5 MBq) injection 48 hours later. (**a**) ^{131}I therapy after NIS-MSC application resulted in a significant delay in tumor growth as compared with the control groups, that were injected with WT-MSC followed by ^{131}I (P = 0.008103; n = 15), with NIS-MSC followed by saline (P = 0.001703; n = 15) or with saline only (n = 15). Immunofluorescence analysis using a Ki67-specific antibody (green) and an antibody against CD31 (red, labeling blood vessels) showed decreased proliferation (Ki67, 25 ± 4.1 %) and reduced blood vessel density (CD31, 1.85 ± 0.25%) in tumors of mice treated with (**b**) NIS-MSC followed by ^{131}I treatment as compared to tumors of mice injected with (**c**) WT-MSC and ^{131}I or mice treated with (**d**) NIS-MSC and saline (Ki67, 45 ± 8.7%; CD31, 5 ± 0.45%). Slides were counterstained with Hoechst Nuclear stain. Magnification ×200.

NIS transduction of prostate cancer cells or local adenoviral *in vivo* *NIS* gene transfer. This approach demonstrated a significant therapeutic effect after application of ^{131}I or alternative radionuclides, such as ^{188}Re and ^{211}At.[14,15,29–32] Our work in the prostate cancer model and subsequent work in other tumor models, including medullary thyroid, colon and hepatocellular cancer,[22,24,25,33–39] have demonstrated the potential of *NIS* as a combined reporter and therapy gene.

One of the major hurdles for safe clinical application of the *NIS* gene-based therapy concept is optimal tumor targeting, with low toxicity, and high transduction efficiency for gene delivery vectors, with the ultimate aim of systemic vector application for the treatment of metastatic disease.

Relatively few studies have investigated NIS-targeted radionuclide therapy of metastatic cancer after systemic *NIS* gene delivery. The application of an oncolytic measles virus or an oncolytic vesicular stomatitis virus in a multiple myeloma mouse model was found to allow the monitoring of virus replication by radioiodine γ-camera or single-photon emission computed tomography (SPECT) imaging as well as stimulation of oncolytic potency of the virus by combination with ^{131}I therapy.[19,40] In a recent study, we used *NIS* as reporter and therapy gene to demonstrate the high potential of synthetic polymeric vectors based on pseudodendritic oligoamines with high intrinsic tumor affinity for tumor-specific delivery of the *NIS* gene. After intravenous application of NIS polyplexes in a syngeneic neuroblastoma mouse model, NIS-mediated radioiodine accumulation was mainly restricted to the tumor, and sufficiently high for a significant delay of tumor growth.[22]

In the current study, we utilized MSCs as gene delivery vehicles for tumor-targeted *NIS* gene delivery in a human hepatocellular cancer xenograft mouse model. Previous studies have shown that MSCs can efficiently migrate and engraft into the tumor stroma of tumor lesions representing the basis for the paradigm of the "Trojan horse" approach in which MSCs are used as shuttle vectors for delivery of therapeutic genes into critical parts of growing tumors.[1,41] In a mouse model it was shown that MSCs expressing TRAIL can provide targeted delivery of this proapoptotic agent to breast cancer metastases to the lung.[9] Similarly, MSCs transduced to express interferon-β or the immunostimulatory chemokine CX3CL1 have been shown to provide an antitumor effect in various murine cancer models, including glioma,[7] breast,[1] melanoma,[10] and colorectal cancer.[11] In two previous studies, we have demonstrated active homing of herpes simplex virus type 1 thymidine kinase-transduced MSCs into primary pancreatic or breast cancer tumor stroma that resulted in significant reduction of tumor growth and in one case reduced incidence of metastases after application of ganciclovir.[8,41]

Here, MSCs stably transfected with *NIS* under control of the cytomegalovirus (CMV) promoter (NIS-MSC) revealed high levels of functional NIS protein expression that resulted in a 55% reduction of survival of HCC cells when cocultured with NIS-MSCs in an ^{131}I *in vitro* clonogenic assay. This demonstrated a significant bystander effect based on the crossfire effect of the β-emitter ^{131}I with a path length of up to 2.4 mm. Following systemic application of NIS-MSCs via the tail vein, 74% of implanted HCC tumors showed tumor-specific ^{123}I accumulation as imaged by γ-camera

scintigraphy with accumulation of ~7–9% ID/g, and a biological half-life of 4 hours. In contrast, control mice showed no tumoral radioiodine uptake, confirming that the observed iodide accumulation in the tumors was mediated by functional NIS expression. *In vivo* ^{123}I-scintigraphic imaging confirmed by *ex vivo* biodistribution experiments revealed significant tumoral radioiodine accumulation. No iodide uptake was measured in nontarget organs, including liver, lungs, spleen or kidneys. Tumoral NIS expression was further verified by quantitative real-time PCR as well as NIS-specific immunoreactivity, which showed expression throughout the tumor stroma with most prominent staining in areas neighboring blood vessels. Interestingly, SV40 large T Ag immunostaining revealed strong accumulation of MSCs in the spleen without detection of NIS-specific immunoreactivity or iodide accumulation. These data suggest that MSCs were recruited to the spleen but did not undergo the same program of differentiation and activation, and therefore did not express the therapeutic gene.

Most of the studies investigating the potential of MSCs as gene delivery vehicles have addressed the issue of biodistribution and tumor-specific recruitment of MSCs mainly by *ex vivo* analysis of reporter gene expression. Our data demonstrate the potential of *NIS* as a dynamic reporter gene offering the possibility of noninvasive *in vivo* tracking of NIS-MSC homing and engraftment at the tumor site by ^{123}I-scintigraphy. This allows a detailed analysis of *in vivo* biodistribution of genetically modified MSCs as well as exact characterization of localization and level of transgene expression, an essential prerequisite for exact planning and monitoring of clinical gene therapy trials.

Our data are consistent with a recently published study by Rad *et al.*[42] who used superparamagnetic iron oxide-labeled NIS-transduced AC133$^+$ progenitor cells to carry the *NIS* gene to sites of breast cancer xenografts in a nude mouse model. After i.v. application progenitor cells were successfully tracked by magnetic resonance imaging, while ^{99m}Tc-SPECT imaging demonstrated *NIS* gene expression at the tumor site confirming tumor-specific recruitment of stem cells.[42] A similar approach was investigated by Loebinger *et al.* who labeled human MSCs with iron oxide nanoparticles, which allowed tracking of MSCs to lung metastases *in vivo* using magnetic resonance imaging.[43] In addition, bioluminescent imaging was used to monitor luciferase-transduced MSC homing and engraftment in a syngeneic breast cancer mouse model.[44]

In addition to ^{123}I γ-camera imaging, we used small animal whole body positron emission tomography (PET) using ^{124}I as radiotracer. Despite the widespread availability of ^{123}I-scintigraphy, PET imaging is attractive for tracking the delivery and tumoral engraftment of NIS-MSCs due to its higher sensitivity and enhanced resolution.[17,27] In addition, fusion of PET with computed tomography images allows a more robust biodistribution analysis and clearly aids in correlative diagnosis in clinical oncology. With translation from animal to human studies in mind, PET/computed tomography could be the optimal method to study MSC biodistribution, followed by quantification of radioiodine accumulation and exact dosimetric calculations. We have demonstrated the feasibility of monitoring MSC biodistribution by ^{124}I-PET allowing a more detailed three-dimensional analysis of NIS-mediated radioiodine accumulation. In support of our data, MSC engraftment and proliferation in tumor stroma of microscopic tumors has successfully be monitored by ^{18}F-FHBG-PET imaging using herpes simplex virus type 1 thymidine kinase as reporter gene.[45]

The ability to monitor MSC distribution effectively sets the stage for therapeutic application of ^{131}I. As detailed above, and shown in the current therapy study, the application of NIS-transduced MSCs allows noninvasive imaging of their recruitment and engraftment at the tumor site, and also provides a powerful anticancer strategy taking advantage of *NIS* as a potent therapy gene. NIS expression allows a significant bystander effect based on the crossfire effect of the β-emitters ^{131}I (path length of up to 2.4 mm) or ^{188}Re (path length of 10 mm) that are both transported by the protein. NIS-mediated uptake of ^{131}I or ^{188}Re in NIS-transduced MSCs therefore can kill neighboring tumor cells, but also can target a significant radiation dose to the tumor stroma, which has been recognized as a crucial and vulnerable target for tumor therapy. Due to its function as a reporter gene, and its association with a significant bystander effect, *NIS* represents an ideal therapy gene in the context of stem cell based gene therapy which was demonstrated in the current study. After three cycles of repetitive MSC injections followed by ^{131}I administration, experimental HCC xenografts showed a significant reduction in tumor growth. In addition, immunofluorescence analysis of tumor tissue showed markedly reduced proliferation and decreased blood vessel density in the NIS-MSC/^{131}I treated mice. To date, only relatively few studies have demonstrated the feasibility of MSCs as gene delivery vehicles for the treatment of malignant tumors. Zischek *et al.* demonstrated significant reduction of pancreatic tumor growth and incidence of metastases using herpes simplex virus type 1 thymidine kinase transfected MSCs after treatment with ganciclovir.[8] In a related study, intratumorally injected TRAIL-secreting umbilical cord blood-derived MSCs significantly reduced tumor growth in a glioma tumor model.[46] However, these studies lack the unique dual function of the *NIS* gene as detailed here.

MSCs are known to have immunosuppressive functions that may influence therapeutic efficacy. We believe that due to the transient nature of the application of the engineered MSCs in concert with the removal of all adoptively applied MSCs in the context of therapy in the current study, and based on our previous studies outlined above, this phenomenon is of minor relevance. A negative effect on therapy was not seen in experiments using syngeneic MSCs expressing a suicide gene in syngeneic immunocompetent mice.[8,41]

In conclusion, our data demonstrate the high potential of genetically engineered MSCs as tumor-selective delivery vehicles for the human *NIS* gene after systemic application. *NIS* as a potent and well characterized reporter gene allowed detailed noninvasive characterization of *in vivo* biodistribution of MSCs by analysis of functional NIS expression by ^{123}I-scintigraphy and ^{124}I-PET imaging, which is an essential prerequisite for exact planning and monitoring of the application of NIS as therapy gene. Moreover, in parallel studies, ^{131}I administration leads to delayed tumor growth. This study therefore opens the exciting prospect of NIS-mediated radionuclide therapy of metastatic cancer taking advantage of the tumor-selective homing of MSCs and the bystander effect of the NIS gene therapy concept.

MATERIALS AND METHODS

Cell culture. The MSCs used express CD73 and CD105, but lack the myelogenic markers CD34, CD14, CD45, and major histocompatibility complex class II and are thus difficult to define.[47,48] A clonal cell line derived from SV40 large T antigen immortalized MSCs from human bone marrow was used for the outlined studies.[48] The cells grow adherently and continuously in cell culture and retain significant pluripotency.[47,48] MSCs were cultured in RPMI (Invitrogen, Life Technologies, Paisley, UK) supplemented with 10% fetal bovine serum (v/v; PAA, Pasching, Austria) and 1% penicillin/streptomycin.

For animal experiments the human hepatocellular carcinoma cell line Huh7 (JCRB 0403) was cultured in DMEM/F12 (Invitrogen, Darmstadt, Germany) supplemented with 10% fetal bovine serum (v/v; PAA), 5% L-Glutamine (Gibco, Karlsruhe, Germany) and 1% penicillin/streptomycin.

For *in vitro* studies, the hepatocellular carcinoma HepG2 cell line (ATCC-HB-8065) was cultured in RPMI (Invitrogen) supplemented with 10% fetal bovine serum (v/v; PAA) and 1% penicillin/streptomycin.

All cell lines were maintained at 37°C and 5% CO_2 in an incubator with 95% humidity.

Stable transfection of mesenchymal stem cells. WT-MSCs were stably transfected with the expression vector CMV-NIS-pcDNA3 (full-length NIS cDNA coupled to the CMV promoter, kindly provided by Dr Jhiang, Ohio State University, Columbus, OH) using LipofectAMINE Plus reagent (Invitrogen) under serum-free conditions according to the manufacturer's recommendations. After transfections, cells were incubated for 24 hours in regular growth medium. Selection was performed with 0.5 mg/ml geneticin (Invitrogen) in RPMI medium containing 10% fetal bovine serum and 1% penicillin/streptomycin. Surviving clones were isolated and subjected to screening for iodide uptake activity (see below). The stably transfected cell line with the highest levels of iodide accumulation among ~60 colonies screened was termed NIS-MSC and used for the experiments.

^{125}I uptake assay. Following transfection, iodide uptake of NIS-MSCs was determined at steady-state conditions as described previously.[32] Results were normalized to cell survival measured by cell viability assay (see below) and expressed as cpm/A 490 nm.

Cell viability assay. Cell viability was measured using the commercially available MTS assay (Promega, Mannheim, Germany) according to the manufacturer's recommendations as described previously.[32]

In vitro *clonogenic assay*. HepG2 cells cocultured with NIS-MSCs or WT-MSCs were incubated for 7 hours with 29.6 MBq (0.8 mCi) ^{131}I in HBSS (Gibco) supplemented with 10 µmol/l NaI and 10 mmol/l HEPES (pH 7.3) at 37 °C. After incubation with ^{131}I, the MSCs were separately removed by incubation with 1% trypsin in phosphate buffered saline (PBS) for 1 minute, which did not affect attachment of HepG2 cells. Thereafter, HepG2 cells were detached by incubation with 0.05% trypsin/0.02% EDTA in PBS for 10 minutes at 37 °C. The HCC cells were then plated at cell densities of 50, 100, 250, 500, 750, 1000 und 2000 cells/well in 12-well plates. Two weeks later, after colony development, cells were fixed with methanol, stained with crystal violet, and HCC colonies containing more than 50 cells were counted. Parallel experiments were performed using HBSS without ^{131}I and all values were adjusted for plating efficiency. The percentage of survival represents the percentage of cell colonies after ^{131}I treatment, compared with mock treatment with HBSS. Purity of HepG2 cells after selective trypsinization was confirmed by phase-contrast microscopy and by immunofluorescence analysis using cell type-specific antibodies (vimentin and keratin) in parallel experiments.

Membrane preparation and western blot analysis. Membrane protein was prepared from NIS-MSCs and WT-MSCs followed by western blot analysis as described previously.[32] A mouse monoclonal NIS-specific antibody (kindly provided by J.C. Morris, Division of Endocrinology, Mayo Clinic and Medical School, Rochester, MN) was applied at a dilution of 1:1,000. As loading controls, the blots were reprobed with a monoclonal antibody directed against β-actin (Sigma, Taufkirchen, Germany).

Establishment of Huh7 xenograft tumors. Huh7 xenograft tumors were established in female CD1 nu/nu mice (Charles River, Sulzfeld, Germany) by subcutaneous injection of 5×10^6 Huh7 cells suspended in 100 µl PBS into the flank region. The animals were maintained under specific pathogen-free conditions with access to mouse chow and water *ad libitum*. The experimental protocol was approved by the regional governmental commission for animals (Regierung von Oberbayern).

***MSC application and radioiodine biodistribution studies* in vivo.** Experiments were initiated when the implanted tumors reached a diameter of 3–5 mm, after a 10-day pretreatment with intraperitoneal injections of 2 µg L-T4/d (Henning, Sanofi-Aventis, Germany), diluted in 100 µl PBS, to suppress thyroidal iodide uptake. WT-MSCs or NIS-MSCs were applied via the tail vein at a concentration of 5×10^5 cells/500 µl. Two groups of mice were established and treated as follows: (i) three i.v. applications of NIS-MSC in four day intervals ($n = 24$); (ii) three i.v. applications of WT-MSC in 4-day intervals ($n = 9$). As an additional control, in a subset of mice injected with NIS-MSC ($n = 9$) the specific NIS-inhibitor sodium-perchlorate ($NaClO_4$, 2 mg per mouse) was injected intraperitoneally 30 minutes prior to ^{123}I administration. Seventy-two hours after the last MSC application, 18.5 MBq (0.5 mCi) ^{123}I was injected intraperitoneally and iodide biodistribution was assessed using a γ-camera equipped with UXHR collimator (Ecam, Siemens, Germany) as described previously.[14,15] Regions of interest were quantified and expressed as a fraction of the total amount of applied radionuclide per gram tumor tissue (after postmortem weighing). The retention time within the tumor was determined by serial scanning after radionuclide injection. Dosimetric calculations were done according to the concept of medical internal radiation dose, with the dosis factor of RADAR-group (http://www.doseinfo-radar.com/).

In an additional group of mice injected with NIS-MSCs ($n = 5$), radioiodine biodistribution was also monitored using ^{124}I-PET imaging after i.v. injection of 20 MBq ^{124}I. PET imaging was performed as described previously.[17,49] In brief, PET data were acquired in list-mode format over 40 minutes on a Siemens Inveon P120 microPET (Siemens Medical Solutions, Munich, Germany). Dynamic emission recordings acquired in list mode were reconstructed using a combined reconstructing algorithm with two OSEM3D iterations as described by Rominger *et al.*[49]

***Analysis of radioiodine biodistribution* ex vivo.** For *ex vivo* biodistribution studies, mice were injected with NIS-MSCs ($n = 8$) or WT-MSCs ($n = 3$) as described above followed by intraperitoneal injection of 18.5 MBq (0.5 mCi) ^{123}I. A subset of NIS-MSC injected mice ($n = 3$) were treated with $NaClO_4$ prior to ^{123}I administration as an additional control. Five hours after ^{123}I injection, mice were killed and organs of interest were dissected, weighed and ^{123}I accumulation was measured in a γ-counter. Results were reported as percentage of injected dose per organ (% ID/organ).

Analysis of NIS mRNA expression using quantitative real-time PCR. Total RNA was isolated from Huh7 tumors or other tissues using the RNeasy Mini Kit (Qiagen, Hilden, Germany) according to the manufacturer's recommendations and quantitative real-time PCR was performed as described previously.[22]

Immunohistochemical analysis of NIS protein and SV40 large T antigen expression. Immunohistochemical staining of paraffin-embedded tissue sections derived from Huh7 tumors after i.v. MSC application was performed as described previously.[25] As primary antibodies, the mouse monoclonal NIS-specific antibody (see above) or the mouse monoclonal anti-SV40 large T Ag antibody (Calbiochem/Merck, Darmstadt, Germany) were used at a dilution of 1:1,000 and 1:2,000, respectively.

***Radioiodine therapy study* in vivo.** Following a 10-day L-T4 pretreatment as described above, two groups of mice were established receiving 55.5 MBq ^{131}I 48 hours after the last of three NIS-MSC (n = 15) or WT-MSC (n = 15) applications in 2-day intervals (each 5×10^5 cells/500 µl PBS), respectively. This cycle was repeated once 24 hours after the last ^{131}I application. Twenty-four hours after these two treatment cycles one additional MSC (5×10^5 cells) injection was administered followed by a third ^{131}I (55.5 MBq) injection 48 hours later. As control, one further group of mice were treated with saline instead of ^{131}I after injection of NIS-MSC (n = 15). A further control group was injected with saline only (n = 15). Tumor sizes were measured before treatment and daily thereafter for up to 7 weeks. Tumor volume was estimated using the equation: tumor volume = length × width × height × 0.52. Mice were killed when tumors started to necrotize, exceed a tumor volume of 1500 mm^3, in case of weight loss of >10%, or impairment of breathing as well as drinking and eating behavior.

Experiments were repeated twice and tumor volumes are expressed as mean of 15 mice per group.

Indirect immunofluorescence assay. Indirect immunofluorescence analysis using a Ki67-specific antibody and an antibody against CD31 was performed on frozen sections as described previously.[14] Immunostainings that had to be compared quantitatively were captured at identical illumination conditions, with identical exposure time and system settings for digital image processing.

Quantification of cellular proliferation (percentage of Ki67 positive cells in the tumor) and blood vessel density (percentage of CD31 positive area in the tumor) was performed by evaluation of 10 high-power fields per tumor (six animals per group) using ImageJ software (NIH, Bethesda, MD).

Results are presented as means ± SD, statistical significance was calculated using Student's t-test.

Statistical methods. All *in vitro* experiments were carried out in triplicates. Results are represented as mean ± SD of triplicates. Statistical significance of *in vitro* experiments was tested using Student's t-test. Statistical significance of *in vivo* experiments has been calculated using Mann–Whitney U test.

ACKNOWLEDGMENTS

We are grateful to J. C. Morris, Division of Endocrinology, Mayo Clinic and Medical School, Rochester, MN for providing the NIS-specific antibody, as well as to S. M. Jhiang, Ohio State University, Columbus, OH for supplying the full-length human NIS cDNA. We also thank Wolfgang Münzing, Cornelia Arszol, Sebastian Nowak and Julia Schlichtiger, Department of Nuclear Medicine, Ludwig-Maximilians-University, Munich, Germany, for their assistance with imaging studies and animal work. This study was supported by grant SFB 824 (Sonderforschungsbereich 824) from the Deutsche Forschungsgemeinschaft, Bonn, Germany to C.S., and by a grant from the Wilhelm-Sander-Stiftung (2008.037.1) to C.S. and P.N. The authors declared no conflict of interest.

REFERENCES

1. Studeny, M, Marini, FC, Dembinski, JL, Zompetta, C, Cabreira-Hansen, M, Bekele, BN *et al.* (2004). Mesenchymal stem cells: potential precursors for tumor stroma and targeted-delivery vehicles for anticancer agents. *J Natl Cancer Inst* **96**: 1593–1603.
2. Fritz, V and Jorgensen, C (2008). Mesenchymal stem cells: an emerging tool for cancer targeting and therapy. *Curr Stem Cell Res Ther* **3**: 32–42.
3. Pittenger, MF, Mackay, AM, Beck, SC, Jaiswal, RK, Douglas, R, Mosca, JD *et al.* (1999). Multilineage potential of adult human mesenchymal stem cells. *Science* **284**: 143–147.
4. Conrad, C, Gupta, R, Mohan, H, Niess, H, Bruns, CJ, Kopp, R *et al.* (2007). Genetically engineered stem cells for therapeutic gene delivery. *Curr Gene Ther* **7**: 249–260.
5. Von Lüttichau, I, Notohamiprodjo, M, Wechselberger, A, Peters, C, Henger, A, Seliger, C *et al.* (2005). Human adult CD34- progenitor cells functionally express the chemokine receptors CCR1, CCR4, CCR7, CXCR5, and CCR10 but not CXCR4. *Stem Cells Dev* **14**: 329–336.
6. Spaeth, EL, Dembinski, JL, Sasser, AK, Watson, K, Klopp, A, Hall, B *et al.* (2009). Mesenchymal stem cell transition to tumor-associated fibroblasts contributes to fibrovascular network expansion and tumor progression. *PLoS ONE* **4**: e4992.
7. Nakamizo, A, Marini, F, Amano, T, Khan, A, Studeny, M, Gumin, J *et al.* (2005). Human bone marrow-derived mesenchymal stem cells in the treatment of gliomas. *Cancer Res* **65**: 3307–3318.
8. Zischek, C, Niess, H, Ischenko, I, Conrad, C, Huss, R, Jauch, KW *et al.* (2009). Targeting tumor stroma using engineered mesenchymal stem cells reduces the growth of pancreatic carcinoma. *Ann Surg* **250**: 747–753.
9. Loebinger, MR, Eddaoudi, A, Davies, D and Janes, SM (2009). Mesenchymal stem cell delivery of TRAIL can eliminate metastatic cancer. *Cancer Res* **69**: 4134–4142.
10. Studeny, M, Marini, FC, Champlin, RE, Zompetta, C, Fidler, IJ and Andreeff, M (2002). Bone marrow-derived mesenchymal stem cells as vehicles for interferon-beta delivery into tumors. *Cancer Res* **62**: 3603–3608.
11. Xin, H, Kanehira, M, Mizuguchi, H, Hayakawa, T, Kikuchi, T, Nukiwa, T *et al.* (2007). Targeted delivery of CX3CL1 to multiple lung tumors by mesenchymal stem cells. *Stem Cells* **25**: 1618–1626.
12. Spitzweg, C and Morris, JC (2002). The sodium iodide symporter: its pathophysiological and therapeutic implications. *Clin Endocrinol (Oxf)* **57**: 559–574.
13. Hingorani, M, Spitzweg, C, Vassaux, G, Newbold, K, Melcher, A, Pandha, H *et al.* (2010). The biology of the sodium iodide symporter and its potential for targeted gene delivery. *Curr Cancer Drug Targets* **10**: 242–267.
14. Willhauck, MJ, Sharif Samani, BR, Gildehaus, FJ, Wolf, I, Senekowitsch-Schmidtke, R, Stark, HJ *et al.* (2007). Application of 188rhenium as an alternative radionuclide for treatment of prostate cancer after tumor-specific sodium iodide symporter gene expression. *J Clin Endocrinol Metab* **92**: 4451–4458.
15. Willhauck, MJ, Samani, BR, Wolf, I, Senekowitsch-Schmidtke, R, Stark, HJ, Meyer, GJ *et al.* (2008). The potential of 211Astatine for NIS-mediated radionuclide therapy in prostate cancer. *Eur J Nucl Med Mol Imaging* **35**: 1272–1281.
16. Dingli, D, Russell, SJ and Morris, JC 3rd (2003). *In vivo* imaging and tumor therapy with the sodium iodide symporter. *J Cell Biochem* **90**: 1079–1086.
17. Groot-Wassink, T, Aboagye, EO, Wang, Y, Lemoine, NR, Reader, AJ and Vassaux, G (2004). Quantitative imaging of Na/I symporter transgene expression using positron emission tomography in the living animal. *Mol Ther* **9**: 436–442.
18. Baril, P, Martin-Duque, P and Vassaux, G (2010). Visualization of gene expression in the live subject using the Na/I symporter as a reporter gene: applications in biotherapy. *Br J Pharmacol* **159**: 761–771.
19. Goel, A, Carlson, SK, Classic, KL, Greiner, S, Naik, S, Power, AT *et al.* (2007). Radioiodide imaging and radiovirotherapy of multiple myeloma using VSV(Delta51)-NIS, an attenuated vesicular stomatitis virus encoding the sodium iodide symporter gene. *Blood* **110**: 2342–2350.
20. Blechacz, B, Splinter, PL, Greiner, S, Myers, R, Peng, KW, Federspiel, MJ *et al.* (2006). Engineered measles virus as a novel oncolytic viral therapy system for hepatocellular carcinoma. *Hepatology* **44**: 1465–1477.
21. Merron, A, Peerlinck, I, Martin-Duque, P, Burnet, J, Quintanilla, M, Mather, S *et al.* (2007). SPECT/CT imaging of oncolytic adenovirus propagation in tumours *in vivo* using the Na/I symporter as a reporter gene. *Gene Ther* **14**: 1731–1738.
22. Klutz, K, Russ, V, Willhauck, MJ, Wunderlich, N, Zach, C, Gildehaus, FJ *et al.* (2009). Targeted radioiodine therapy of neuroblastoma tumors following systemic nonviral delivery of the sodium iodide symporter gene. *Clin Cancer Res* **15**: 6079–6086.
23. Trujillo, MA, Oneal, MJ, McDonough, S, Qin, R and Morris, JC (2010). A probasin promoter, conditionally replicating adenovirus that expresses the sodium iodide symporter (NIS) for radiovirotherapy of prostate cancer. *Gene Ther* **17**: 1325–1332.
24. Willhauck, MJ, Sharif-Samani, B, Senekowitsch-Schmidtke, R, Wunderlich, N, Göke, B, Morris, JC *et al.* (2008). Functional sodium iodide symporter expression in breast cancer xenografts *in vivo* after systemic treatment with retinoic acid and dexamethasone. *Breast Cancer Res Treat* **109**: 263–272.
25. Spitzweg, C, Baker, CH, Bergert, ER, O'Connor, MK and Morris, JC (2007). Image-guided radioiodide therapy of medullary thyroid cancer after carcinoembryonic antigen promoter-targeted sodium iodide symporter gene expression. *Hum Gene Ther* **18**: 916–924.
26. Carlson, SK, Classic, KL, Hadac, EM, Dingli, D, Bender, CE, Kemp, BJ *et al.* (2009). Quantitative molecular imaging of viral therapy for pancreatic cancer using an engineered measles virus expressing the sodium-iodide symporter reporter gene. *AJR Am J Roentgenol* **192**: 279–287.
27. Dingli, D, Kemp, BJ, O'Connor, MK, Morris, JC, Russell, SJ and Lowe, VJ (2006). Combined I-124 positron emission tomography/computed tomography imaging of NIS gene expression in animal models of stably transfected and intravenously transfected tumor. *Mol Imaging Biol* **8**: 16–23.
28. Wapnir, IL, Goris, M, Yudd, A, Dohan, O, Adelman, D, Nowels, K *et al.* (2004). The Na+/I- symporter mediates iodide uptake in breast cancer metastases and can be selectively down-regulated in the thyroid. *Clin Cancer Res* **10**: 4294–4302.
29. Kakinuma, H, Bergert, ER, Spitzweg, C, Cheville, JC, Lieber, MM and Morris, JC (2003). Probasin promoter (ARR(2)PB)-driven, prostate-specific expression of the human sodium iodide symporter (h-NIS) for targeted radioiodine therapy of prostate cancer. *Cancer Res* **63**: 7840–7844.
30. Spitzweg, C, Dietz, AB, O'Connor, MK, Bergert, ER, Tindall, DJ, Young, CY *et al.* (2001). *In vivo* sodium iodide symporter gene therapy of prostate cancer. *Gene Ther* **8**: 1524–1531.
31. Spitzweg, C, O'Connor, MK, Bergert, ER, Tindall, DJ, Young, CY and Morris, JC (2000). Treatment of prostate cancer by radioiodine therapy after tissue-specific expression of the sodium iodide symporter. *Cancer Res* **60**: 6526–6530.
32. Spitzweg, C, Zhang, S, Bergert, ER, Castro, MR, McIver, B, Heufelder, AE *et al.* (1999). Prostate-specific antigen (PSA) promoter-driven androgen-inducible expression of sodium iodide symporter in prostate cancer cell lines. *Cancer Res* **59**: 2136–2141.
33. Scholz, IV, Cengic, N, Baker, CH, Harrington, KJ, Maletz, K, Bergert, ER *et al.* (2005). Radioiodine therapy of colon cancer following tissue-specific sodium iodide symporter gene transfer. *Gene Ther* **12**: 272–280.
34. Dwyer, RM, Bergert, ER, O'connor, MK, Gendler, SJ and Morris, JC (2005). *In vivo* radioiodide imaging and treatment of breast cancer xenografts after MUC1-driven expression of the sodium iodide symporter. *Clin Cancer Res* **11**: 1483–1489.

35. Dwyer, RM, Schatz, SM, Bergert, ER, Myers, RM, Harvey, ME, Classic, KL *et al.* (2005). A preclinical large animal model of adenovirus-mediated expression of the sodium-iodide symporter for radioiodide imaging and therapy of locally recurrent prostate cancer. *Mol Ther* **12**: 835–841.
36. Hervé, J, Cunha, AS, Liu, B, Valogne, Y, Longuet, M, Boisgard, R *et al.* (2008). Internal radiotherapy of liver cancer with rat hepatocarcinoma-intestine-pancreas gene as a liver tumor-specific promoter. *Hum Gene Ther* **19**: 915–926.
37. Li, H, Peng, KW, Dingli, D, Kratzke, RA and Russell, SJ (2010). Oncolytic measles viruses encoding interferon beta and the thyroidal sodium iodide symporter gene for mesothelioma virotherapy. *Cancer Gene Ther* **17**: 550–558.
38. Peerlinck, I, Merron, A, Baril, P, Conchon, S, Martin-Duque, P, Hindorf, C *et al.* (2009). Targeted radionuclide therapy using a Wnt-targeted replicating adenovirus encoding the Na/I symporter. *Clin Cancer Res* **15**: 6595–6601.
39. Willhauck, MJ, Sharif Samani, BR, Klutz, K, Cengic, N, Wolf, I, Mohr, L *et al.* (2008). Alpha-fetoprotein promoter-targeted sodium iodide symporter gene therapy of hepatocellular carcinoma. *Gene Ther* **15**: 214–223.
40. Dingli, D, Peng, KW, Harvey, ME, Greipp, PR, O'Connor, MK, Cattaneo, R *et al.* (2004). Image-guided radiovirotherapy for multiple myeloma using a recombinant measles virus expressing the thyroidal sodium iodide symporter. *Blood* **103**: 1641–1646.
41. Conrad, C, Hüsemann, Y, Niess, H, von Luettichau, I, Huss, R, Bauer, C *et al.* (2011). Linking transgene expression of engineered mesenchymal stem cells and angiopoietin-1-induced differentiation to target cancer angiogenesis. *Ann Surg* **253**: 566–571.
42. Rad, AM, Iskander, AS, Janic, B, Knight, RA, Arbab, AS and Soltanian-Zadeh, H (2009). AC133+ progenitor cells as gene delivery vehicle and cellular probe in subcutaneous tumor models: a preliminary study. *BMC Biotechnol* **9**: 28.
43. Loebinger, MR, Kyrtatos, PG, Turmaine, M, Price, AN, Pankhurst, Q, Lythgoe, MF *et al.* (2009). Magnetic resonance imaging of mesenchymal stem cells homing to pulmonary metastases using biocompatible magnetic nanoparticles. *Cancer Res* **69**: 8862–8867.
44. Klopp, AH, Spaeth, EL, Dembinski, JL, Woodward, WA, Munshi, A, Meyn, RE *et al.* (2007). Tumor irradiation increases the recruitment of circulating mesenchymal stem cells into the tumor microenvironment. *Cancer Res* **67**: 11687–11695.
45. Hung, SC, Deng, WP, Yang, WK, Liu, RS, Lee, CC, Su, TC *et al.* (2005). Mesenchymal stem cell targeting of microscopic tumors and tumor stroma development monitored by noninvasive *in vivo* positron emission tomography imaging. *Clin Cancer Res* **11**: 7749–7756.
46. Kim, SM, Oh, JH, Park, SA, Ryu, CH, Lim, JY, Kim, DS *et al.* (2010). Irradiation enhances the tumor tropism and therapeutic potential of tumor necrosis factor-related apoptosis-inducing ligand-secreting human umbilical cord blood-derived mesenchymal stem cells in glioma therapy. *Stem Cells* **28**: 2217–2228.
47. Conrad, C, Gottgens, B, Kinston, S, Ellwart, J and Huss, R (2002). GATA transcription in a small rhodamine 123(low)CD34(+) subpopulation of a peripheral blood-derived CD34(-)CD105(+) mesenchymal cell line. *Exp Hematol* **30**: 887–895.
48. Thalmeier, K and Huss, R (2001). Highly efficient retroviral gene transfer into immortalized CD34(-) cells and organ distribution after transplantation into NOD/SCID mice. *Cytotherapy* **3**: 245–251.
49. Rominger, A, Wagner, E, Mille, E, Böning, G, Esmaeilzadeh, M, Wängler, B *et al.* (2010). Endogenous competition against binding of [(18)F]DMFP and [(18)F] fallypride to dopamine D(2/3) receptors in brain of living mouse. *Synapse* **64**: 313–322.